Available online at www.sciencedirect.com

ScienceDirect

journal homepage: www.elsevier.com/locate/he

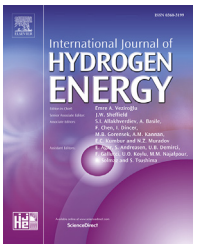

Power generation performance of hydrogen-fueled micro thermophotovoltaic reactor

Yueh-Heng Li [a,b,*], Jing Ru Hong [a]

[a] Department of Aeronautics and Astronautics, National Cheng Kung University, Tainan, 701, Taiwan, ROC
[b] Research Center for Energy Technology and Strategy, National Cheng Kung University, Tainan, 701, Taiwan, ROC

ARTICLE INFO

Article history:
Received 5 August 2017
Received in revised form
18 November 2017
Accepted 4 December 2017
Available online 20 December 2017

Keywords:
Catalytic combustion
Platinum
Small-scale reactor
Thermophotovoltaic
Heterogeneous and homogeneous reaction

ABSTRACT

A tubular platinum reactor with a perforated annular array enables fuel/air mixtures to exchange sides, thus sustaining flames and preventing heat loss. Consequently, the combustion efficiency and operational range can be enhanced. A hydrogen/air mixture was introduced into inner and outer chambers at different equivalence ratios and flow velocities to chemically and physically investigate the interplay between the chambers. The benefits of hydrogen include a high gravimetric heating value, flame speed, and diffusion capacity and short chemical reaction time. The coexistence of heterogeneous (surface) and homogeneous (gas) reactions in the micro TPV reactor was examined and elucidated in terms of aerodynamics, mass and heat transfer, and chemical reactivity. Furthermore, a TPV reactor with TPV cell arrays was assembled, and the corresponding radiant efficiency of the emitter and the overall efficiency of the proposed micro TPV system were determined in this study.

Introduction

The proliferation of microelectromechanical systems and their demand for miniature power sources, ranging from 10 to 1000 W/kg [1], have accelerated the development of miniature power. In general, power systems employing hydrogen or hydrocarbon fuels provide much higher energy density according to specific mass compared with traditional systems [2,3]. A series of combustion-based micro power systems have been successfully prototyped, including the micro gas turbine [4], micro-free-piston engine [5], micro thermoelectric device [6] and micro thermophotovoltaic (TPV) system [7–9]. Although their current efficiency is low, these micro systems have exhibited the potential to generate power in the order of a few watts within a volume of several cubic centimeters. The micro-TPV power generator is a typical direct energy conversion device that uses PV cells to convert heat radiation, from the combustion of fossil fuels, into electricity [10,11]. It does not include any moving parts; therefore, its fabrication and assembly are relatively easy. Unlike solar photovoltaics, TPV cells are illuminated by combustion-driven radiation sources. Because these sources can provide a radiant power density much greater than that of the sun, the electric power density of TPV cells is much higher than that of solar cells. Accordingly, understanding the fundamental characteristics of combustion in the micro scale is the key to improving the system efficiency and optimizing the design.

A reduction in combustor volume results in substantial heat loss and radical destruction on the combustor wall. Some

* *Corresponding author*. Department of Aeronautics and Astronautics, National Cheng Kung University, Tainan, 701, Taiwan, ROC.
E-mail address: yueheng@mail.ncku.edu.tw (Y.-H. Li).
https://doi.org/10.1016/j.ijhydene.2017.12.035
0360-3199/

research groups have applied combustion-enhancing methods such as external heating to overcome the heat loss problem, whereas others have experimented with catalyzed combustion to minimize the radical quenching effect. A backward-facing step in a millimeter-sized cylindrical tube is employed to control the flame position. This cost-effective configuration has been used as a heat source for micro-TPV systems [12,13]. To maximize the output of the micro-TPV generator, a high wall temperature and uniform distribution are of primary concern. Sui et al. [14] pointed out that the appropriate flow structure design can improve the spatial uniformity of surface temperature. Reducing wall thickness and step height gives rise to a higher wall temperature. For instance, Pan et al. [15] discussed the effects of major micro-combustor parameters on the radiation intensity in micro-TPV system, fuel to oxygen ratio, nozzle to combustor diameter ratio, and wall thickness to combustor diameter ratio. Furthermore, porous media combustion occurs in a three-dimensional solid porous matrix having interconnected pores. This enhances the heat transfer from the burned hot gas to the unburnt mixture through conduction, convection, and radiation. In addition, catalytic micro combustors exhibit wider stability than that of homogeneous micro combustors [16–18]. Using numerical simulation, Li et al. [19,20] investigated heterogeneous and homogeneous mechanisms of hydrocarbon fuels combustion enhancement through catalyst segmentation with cavities in a micro reactor. The catalyst induced an exothermic homogeneous reaction near the following non-catalytic wall or cavity. The cavities in the small-scale reactor effectively reduced flame instability and enhanced flammability. Yang et al. [21] testified the output electrical power of the system with platinum wall increased by 11–23.8% compared with that without platinum. Sui and Mantzaras [22]concluded that blowout limits of fuel-lean hydrogen/air mixture in platinum coated micro-channels could not be reached even for inlet velocities as high as 80 m/s at 1 bar.

In recent years, many scholars have focused on applying TPV power systems as portable devices. Li et al. [23] and Yang et al. [24] proposed a hydrogen-fueled micro TPV combustor and used a backward-facing step as a flame stabilization mechanism to control the flame position. Li et al. [25] studied TPV power extensively, converting flame radiation into electrical output by using PV cells. Jiang et al. [26] corroborated a micro-combustor with baffles to apparently extend the blowout limit and enhance the combustion and radiant efficiency. Park et al. [27] proposed a heat-recirculating micro-emitter and its power ranges from 1 to 10 W. Lei et al. [28] designed a micro-combustor with heat recirculation and achieved the extension of flammability. Qiu and Hayden [10] demonstrated a novel cascading TPV and TE power generation system. Yang et al. [29] discussed the factors affecting the combustor of a TPV power system, which include the fuel ratio, flow velocity, and dimensions of the burner exit.

Regrading to the improvement of TPV power output, the use of spectral-control technique for tailoring the radiation spectrum emitted onto the TPV system is prevailing. A selective emitter capitalizes on suppressing the emission of sub-bandgap photons. Similarly, a selective filter benefits from transmitting convertible photons while reflecting low energy photons back to the emitter. Owing to complex fabrication processes and expensive cost of selective emitters and filters, the emitter material in a typical TPV power system is usually silicon carbide (SiC). It emits blackbody radiation (emissivity $\fallingdotseq$ 0.9) and is resistant to high temperature. However, the radiation spectrum of SiC is broadband. According to the Stefan–Boltzmann law, a higher emitter surface temperature leads to higher power output. Therefore, a means for increasing the temperature of the reactor is required. Yang et al. [30] tested different emitting materials for enhancing radiation efficiency. In addition, quartz enables to provide optical transmission from near-ultraviolet to mid-infrared wavelength, and it is effective filter to block low-energy photons [31]. Accordingly, quartz tube acts like a band-pass filter to trap thermal radiation inside the chamber and enhance the chamber temperature. Li et al. [32] proposed a metal-oxide-deposited quartz emitter. This emitter pertains a semi-transparent chamber to allow the portion of radiation emitting outward the chamber and low-energy radiation reflecting back inward the chamber.

In previous papers [23,25], a platinum tube with a perforated ring and fuel/air mixture deployment conditions was testified to overcome the problems of combustion instability and radical termination in a small space. Compared to a plain platinum tube, a perforated platinum tube with a backward-facing step apparently enhances flame stabilization and extends stable flammability. In this study, a micro TPV reactor was fueled with hydrogen due to inherent advantages of high gravimetric heating value, flame speed, and diffusion capacity. The interaction between the inner and outer chambers was experimentally and numerically investigated with regards to the effect of fuel concentration and flow velocity. The coexistence of heterogeneous (surface) and homogeneous (gas) reactions in the micro TPV reactor was examined in terms of aerodynamics, mass and heat transfer, and chemical reactivity. Finally, a TPV reactor with PV cell arrays was assembled, and the corresponding radiant efficiency of the emitter and the overall efficiency of the proposed micro TPV system are determined.

Experimental apparatus

Fig. 1 shows a schematic diagram of the micro TPV reactor, which consists of a platinum tube with dimensions of 5.3 mm (ID) × 6 mm (OD) × 30 mm (L) and a quartz tube with dimensions of 8 mm (ID) × 10 mm (OD) × 160 mm (L). The quartz tube is mounted outside the platinum tube. Eight perforation holes (1 mm in diameter) are equidistantly placed around the platinum tube at a distance of 5 mm from the bottom. The platinum tube is mounted on the flange of a stainless steel tube, which measures 4 mm in ID and 5.3 mm in OD. It features a backward-facing step, the length of which is 1 mm, in the connection section. The experiment involved introducing fuel at different equivalence ratios and compositions into the inner and outer chambers to investigate the flame behavior in the micro combustor. The flame behavior was recorded using the Nikon D80 with the aperture and exposure time fixed at F5.6 and 1/100, respectively, for all photographs. The wall temperature of the micro TPV reactor was measured using an

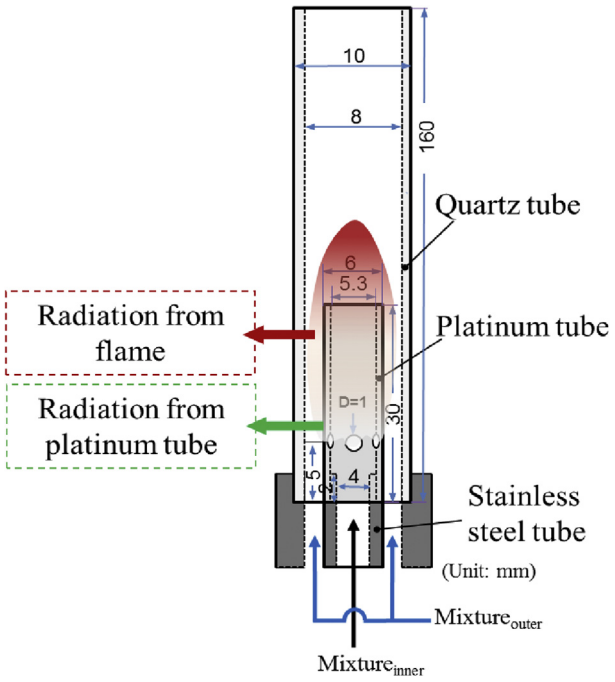

Fig. 1 – The schematic diagram of micro TPV reactor.

infrared thermometer (model RAYMA2SCCFL, Raytek Company), and gas chromatography was performed to analyze the composition of the flue gas.

In general, a single radiometer is used to gauge the irradiance of an emitter at specific location, and to determine the overall irradiance of the micro-TPV reactor by multiplying with incandescent surface area under the assumption of uniform incandescence over the emitter. However, perturbations of combustion and fluid dynamics may lead to non-uniformity of the TPV radiation. Therefore, to mitigate the uncertainty of irradiating measurement, the proposed micro-TPV reactor was, for the first time, placed in the center of the integrating sphere. As the radiation of the combustor scattered uniformly, the optical fiber collected the radiation in the integrating sphere and sent the signal to the spectral meter to measure the irradiance. An integrating sphere connected to a spectrometer (USB2000 + XR, Ocean Optic Inc.) was employed to measure the irradiation of the emitter, as shown in Fig. 2. The integrating sphere was 15 cm in diameter, and magnesium oxide was deposited on the inner surface. The spectrometer covers wavelengths from 200 to 1050 nm. The emitter was placed in the center of the integrating sphere so that the emitting radiation would scatter and be distributed uniformly on the surface of the sphere. The spectrometer was connected to the integrating sphere to obtain the radiation flux. By multiplying the outer surface area of the emitter, the total irradiation could be determined.

In addition, a monochromator (DK240, Spectral Products Company) with an IR photoresistor (AD131-USB, Spectral Products Company) was employed to measure the spectral distribution of the emitter. The scanning spectrum of the monochromator ranges from 400 to 1500 nm. The IR photoresistor was a convenient computer-controlled photoresistor connected to the monochromator. The radiation was collected and introduced to the monochromator by a convex lens set, and the spectral distribution of radiation was determined using the IR photoresistor.

Combustion characteristics of micro TPV reactor

Effect of fuel concentration

In a previous study [23], numerical results demonstrated that the existence of a gap in a segmented platinum tubular reactor can facilitate the induction of a catalytically stabilized thermal (CST) gas reaction in a confined tube. The gap not only provides a low-velocity region to stabilize flames but also enables the flow of fuels and radicals from the outer chamber to the inner chamber. The interaction between the inner and outer chambers was investigated according to the effects of aerodynamics, mass and heat transfer, and chemical reactivity. To examine the minimal fuel concentration required for inducing a CST gas reaction, the fuel/air mixture was deliberately introduced into the inner or outer chamber only and the other chamber was filled with air, representing an equivalence ratio of 0. Fig. 3 depicts the flame modes for different equivalence ratios in the inner chamber and the pure air condition in the outer chamber, whereas Fig. 4 illustrates those for the opposite fuel/air deployment conditions. Depending on the fuel/air condition and flow velocity, there are four flame modes, the CST gas reaction, a surface reaction, flash back, and no reaction. The flame mode of the CST gas reaction involves the coexistence of heterogeneous (surface) and homogeneous (gas) reactions, and the gas reaction is sustained by inheriting radicals and thermal energy from the

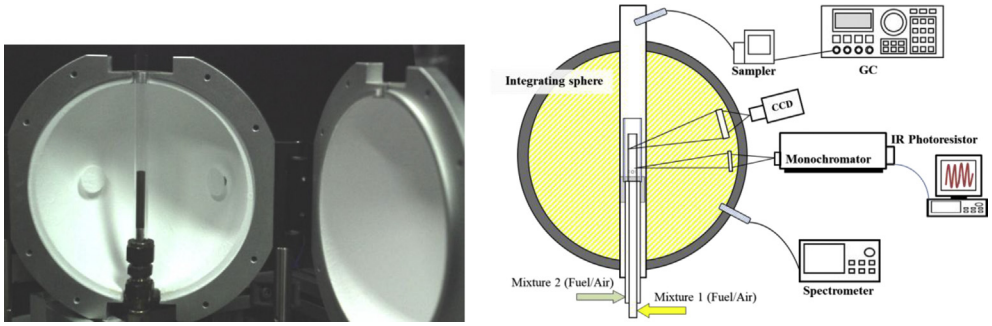

Fig. 2 – The photograph of the integrating sphere assembling with the spectrometer.

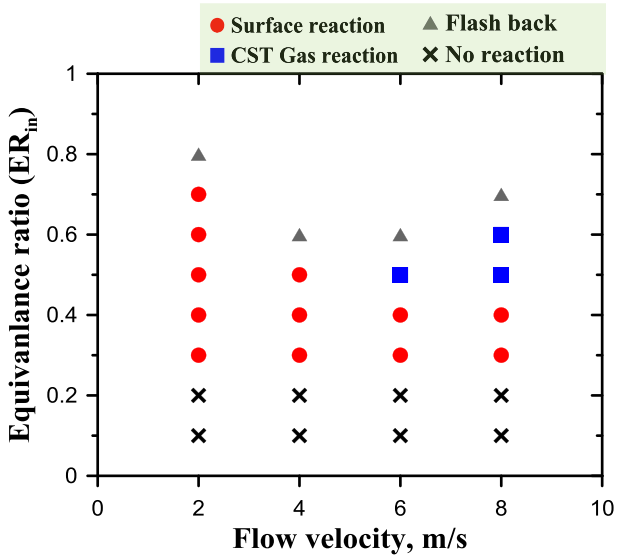

Fig. 3 – The flame modes in the case of different equivalence ratios in the inner chamber and pure air condition in the outer chamber.

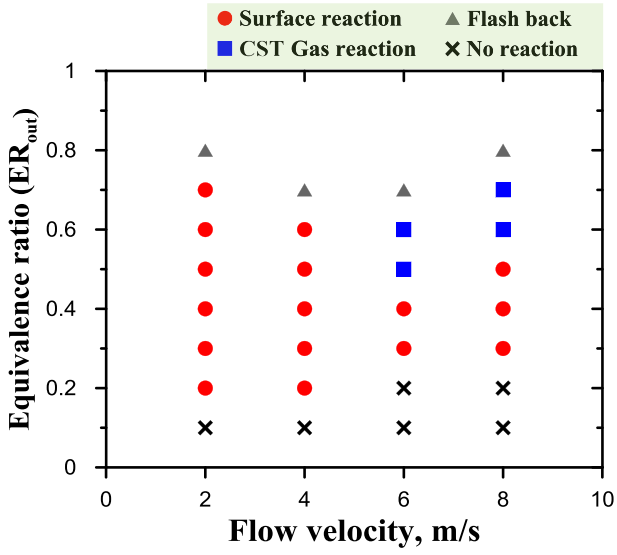

Fig. 4 – The flame modes in the case of different equivalence ratios in the outer chamber and pure air condition in the inner chamber.

surface reaction. Fig. 3 illustrates that the surface reaction is generated in the inner chamber at an ER_{in} of 0.3 and ER_{out} of 0. Subsequently, when ER_{in} rises to 0.5 at the fixed inlet velocity of 6 m/s, the CST gas reaction occurs. By contrast, when only air is delivered into the inner chamber, the surface reaction is initiated at the ER_{out} of 0.3 and the fixed inlet velocity of 6 m/s, and the CST gas reaction is sustained at the ER_{out} of 0.5, as shown in Fig. 4. For flow rates are 2 and 4 m/s, surface reaction occurs in Fig. 4 at $ER_{out} = 0.2$, in Fig. 3 a higher $ER_{in} = 0.3$ is needed. This is counterintuitive, since it is stated that combustion in the outer annulus has more heat losses. Therefore, Fig. 3 should have expected better combustion stability, not Fig. 4 in cases of low flow velocity. However, the ratio of catalytic surface to volume (CS/V) is concerned. The inner tube has a CS/V of 0.377 mm^{-1}, while the outer annulus has a larger CS/V of 0.43 mm^{-1}. The larger CS/V of the outer annulus favors catalytic surface reactions more than the lower CS/V of the inner tube. The operating ranges of the surface and CST gas reactions in Fig. 4 are apparently wider than those in Fig. 3. These results indicate that when the surface reaction or CST gas reaction is sustained in the outer chamber, most of the released heat is lost to the ambient through the quartz wall via thermal radiation, whereas when the surface reaction or CST gas reaction is sustained in the inner chamber, the radiation from the inner chamber heats the incoming unburnt gas mixture and maintains a high gas temperature inside the inner chamber. Accordingly, the minimal equivalence ratio required for sustaining the CST gas reaction in the inner chamber is 0.5 because of low heat loss in the inner chamber compared with the outer chamber. According to the results in Figs. 3 and 4, the equivalence ratio for the inner chamber can be fixed at 0.3 to induce the surface reaction, whereas the equivalence ratio for the outer chamber can be fixed at 0.5 to induce the CST gas reaction. Thus, a combustion characteristic of this study was to use the heat and radicals from the inner chamber to facilitate the inception of the gas reaction in the outer chamber. The minimal equivalence ratio required to induce the surface reaction was set to 0.3 for the following experiments.

To determine the effect of fuel deployment on combustion characteristics, the illumination behaviors of a micro TPV reactor under various fuel deployment conditions at a fixed flow velocity of 6 m/s in the inner and outer chambers were analyzed, as shown in Fig. 5. The equivalence ratio of one chamber was fixed at 0.3, whereas the other chamber had various equivalence ratios ranging from 0.1 to 0.5. When the ER_{in} is fixed at 0.3, the micro TPV reactor exhibits dim red illumination at an ER_{out} of 0.1 or 0.2, evidencing that only the surface reaction occurs. When ER_{out} rises to 0.3 or higher, the CST gas reaction occurs in the outer chamber. Relatively

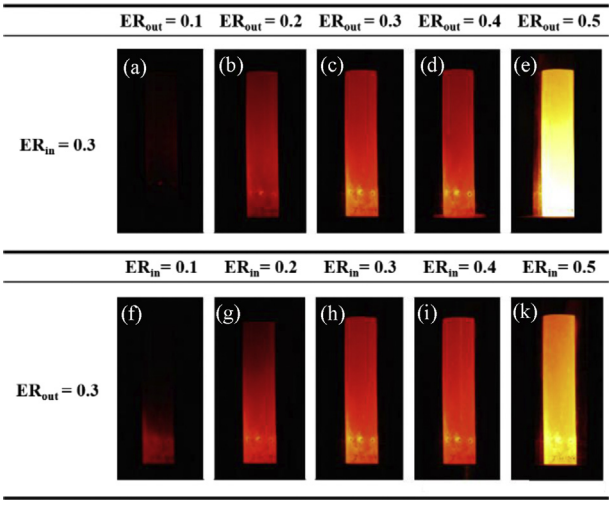

Fig. 5 – Illumination behaviors of the micro-TPV reactor in various fuel deployments and fixed flow velocity of 6 m/sec.

bright yellow illumination rimming the perforations is evident, revealing the presence of the CST gas reaction anchored to the holes. When ER_{out} rises to 0.5, the TPV reactor exhibits extremely bright illumination on the surface. Similarly, when ER_{out} is fixed at 0.3, only the surface reaction occurs at ER_{in} values lower than 0.3, but the CST gas reaction is present at ER_{in} values greater than or equal to 0.3. Particularly, the luminescence when ER_{in} is 0.3 and ER_{out} is 0.5 (case e in Fig. 5) is stronger than that when ER_{out} is 0.3 and ER_{in} is 0.5 (case j in Fig. 5). Fig. 6 shows the measured surface temperature along the outer surface of the micro TPV reactor when ER_{in} is 0.3 and ER_{out} is 0.5, and when ER_{in} is 0.5 and ER_{out} is 0.3. Notably, relatively high surface temperatures are concentrated in the upstream section, close to the holes, when ER_{in} is 0.3 and ER_{out} is 0.5, whereas the surface temperature distribution becomes narrower but more uniform when ER_{in} is 0.5 and ER_{out} is 0.3. Apparently, the combustion characteristics and flame stabilization mechanism of the micro TPV reactor in these two conditions are distinct, resulting in different luminous intensities and temperature distributions. In addition, the temperature distributions of these two conditions are not uniform. The surface temperature standard deviations in the case of $ER_{in} = 0.3/ER_{out} = 0.5$ is 107.6 k, less than 129.5 k in the case of $ER_{in} = 0.5/ER_{out} = 0.3$. It means the luminescent uniformity in the case of $ER_{in} = 0.3/ER_{out} = 0.5$ is better than the case of $ER_{in} = 0.5/ER_{out} = 0.3$.

To determine the effect of fuel deployment on the chemical reactivity of the micro TPV reactor, a simplified simulation was performed. A commercial code, CFD-ACE+, was modified to incorporate detailed gas-phase and surface reaction mechanisms in CHEMKIN formats for the simulation. For simplicity, the small-scale combustor was modeled as a two-dimensional system. The simplified micro TPV combustor consists of two platinum tube segments with a gap of 1 mm; the dimensions are 5.3 mm (ID) × 6 mm (OD) × 4.5 mm (L) for the upstream tube and 5.3 mm (ID) × 6 mm (OD) × 44.5 mm (L) for the downstream tube. The platinum tubes are coaxially placed in a quartz tube, of which the dimensions are 8 mm (ID) × 10 mm (OD) × 50 mm (L), and this coaxial reactor comprises central (inner) and annulus (outer) chambers. H_2–air mixtures were individually introduced into the inner and outer chambers of the TPV reactor at different equivalence ratios. The inlet temperature was 300 K, and a uniform velocity profile (6 m/s) was specified at the inlet. The thermal conductivity of quartz tube is 6 W/m-k, and that of platinum tube is 78 W/m-k. For the thermal boundary at the outer surface of quartz tube, the heat lost to the ambient (300 k) was due to heat convention by air, described as: $q'' = h(T_w - 300)$, where h is the heat transfer coefficient (20 $W/m^2/k$) and T_w is the wall temperature. At the exit, a constant ambient pressure of 101 kPa was specified and an extrapolation scheme was used for determining species and temperature. Chemical reaction mechanisms were used in the gas phase as well as on the catalyst surface. The homogeneous reaction mechanism proposed by Miller and Bowman [33], which consists of nine species and 19 reaction steps, was used for hydrogen–air combustion. The surface reaction mechanism was constructed primarily on the basis of that proposed by Deutschmann et al. [34]. These reaction mechanisms have been used in previous studies and comparisons with experimental results were satisfactory [19,23].

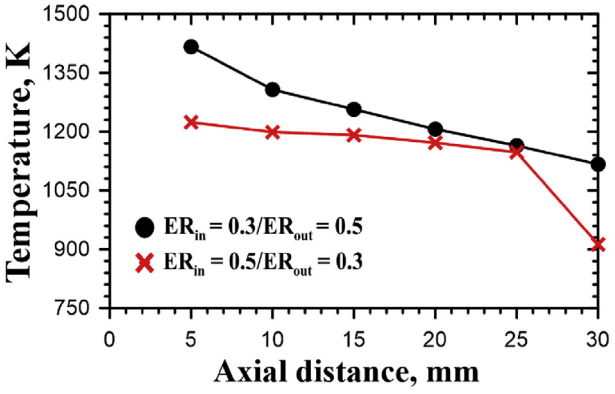

Fig. 6 – Surface temperatures along the micro-TPV reactor under the different fuel deployments.

Fig. 7 depicts the distributions of temperature with overlaid velocity vectors and velocity magnitude level lines for (a) an ER_{in} of 0.5 and an ER_{out} of 0.3, and (b) an ER_{in} of 0.3 and an ER_{out} of 0.5 at the fixed inlet velocity of 6 m/s within the first 1 cm from the inlet. Fig. 8 illustrates the distribution of the OH mass fraction with overlaid local equivalence ratio (LER) level lines for (a) an ER_{in} of 0.5 and ER_{out} of 0.3, and (b) an ER_{in} of 0.3 and ER_{out} of 0.5. According to Fig. 7, the velocity vectors in the vicinity of the gap flow from the outer chamber to the inner chamber, even when the initial inlet velocities in the two chambers are identical. In general, the fuel/air mixture induces the surface reaction in the upstream segment because of the relatively high mass diffusion capability of hydrogen and generates thermal expansion of the mixture gas. However, the space of the outer chamber is much narrower than that of the inner chamber, even though the cross-sectional areas of the chambers are identical. The localized pressure difference between the two sides of the gap induces a drag force, which contributes in driving the fuel/air mixture from the outer chamber to the inner chamber, simultaneously increasing the LER in the inner chamber but reducing the LER

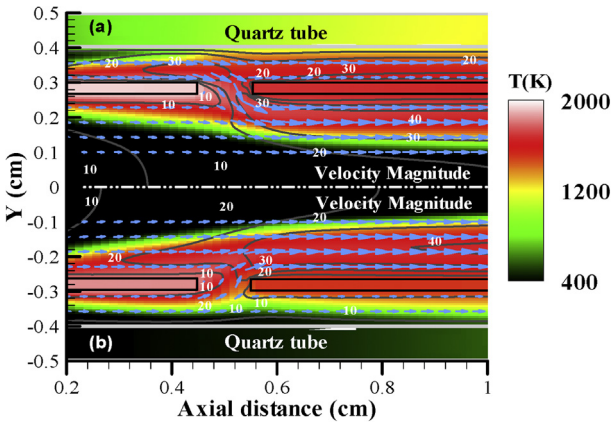

Fig. 7 – The distributions of temperature with overlaid velocity vectors and velocity magnitude level lines for the cases of (a) $ER_{in} = 0.3/ER_{out} = 0.5$, and (b) $ER_{in} = 0.5/ER_{out} = 0.3$, respectively, in the fixed inlet velocity of 6 m/sec in first 1 cm distance away from the inlet.

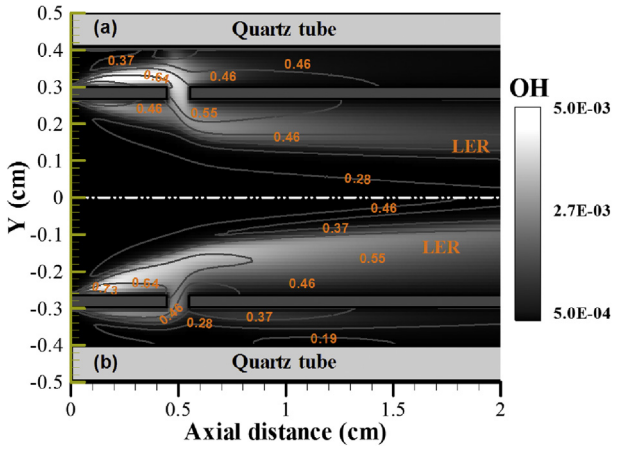

Fig. 8 – The distributions of OH mass fractions with overlaid velocity vectors and local equivalence ratio level lines for the cases of (a) $ER_{in} = 0.3/ER_{out} = 0.5$, and (b) $ER_{in} = 0.5/ER_{out} = 0.3$, respectively, in the fixed inlet velocity of 6 m/sec in first 2 cm distance away from the inlet.

in the outer chamber. Alternatively, the pressure drop in the two combustion chambers is dominated by the surface to volume ratio (S/V). The S/V of the inner platinum tube is 0.377 mm^{-1}, while the S/V of the outer chamber is 1 mm^{-1}. Hence, the much larger S/V of the annulus will create a larger pressure drop due to wall friction. Accordingly, the far-upstream pressure in the initial part of the annulus would be higher than the corresponding pressure in the inner tube. This in turn drives the flow towards the inner tubular reactor. Fig. 8a shows that OH radicals are generated in large quantities along the outer surface of the upstream platinum tube, and meanwhile, intense OH radical concentration occurs on the gap, trailing toward the inner chamber. This observation reveals that the CST gas reaction is sustained on the outer surface of the upstream platinum tube and then contributes in accelerating the flow of the mixture in the outer chamber into the inner chamber. Furthermore, the LER along the inner chamber of the downstream platinum tube increases because of hydrogen flowing in the inner chamber and increasing the LER. By inheriting thermal energy and radicals from the upstream section, the CST gas reaction is generated and sustained in the holes and trails toward the inner and outer chambers. Characteristically, a mixture with a relatively high equivalence ratio in the outer chamber can induce the CST gas reaction along the outer surface of the upstream platinum tube, and unburnt fuels and radicals are then driven into the inner chamber through the gap to facilitate the gas reaction in the inner chamber. By contrast, Fig. 8b presents massive OH radical generation in the inner chamber of the upstream platinum tube and mild OH radical concentration on the outer surface of the upstream platinum tube. Compared with the magnitude of velocity vectors in the vicinity of the gap in Fig. 7a, that of the velocity vectors directed toward the inner chamber decreases in Fig. 7b because thermal expansion of gas is reduced in the outer chamber. Accordingly, a mixture with a relatively low equivalence ratio in the outer chamber could generate a mild chemical reaction along the outer surface of the upstream platinum tube and reduce flow-driven force in the outer chamber. The tendency of unburnt fuels to be drawn to the inner chamber lowers the concentration of remaining fuel in the outer chamber. Therefore, insufficient heat release and the remaining fuel cannot sustain the consequent chemical reaction in the downstream segment of the outer chamber.

Fig. 9 depicts the operating ranges for (a) various ER_{out} values and a fixed ER_{in}, and (b) various ER_{in} values and a fixed ER_{out}. The experimental results show that the operating range of the CST gas reaction is wider for various ER_{in} values and a fixed ER_{out} of 0.3 than for various ER_{out} values and a fixed ER_{in} of 0.3. When ER_{in} and ER_{out} are 0.3 and the flow rate is equal to or more than 6 m/s, the CST gas reaction can be induced and sustained in the micro TPV reactor. Flames can be sustained in either the holes of the platinum tube or the backward-facing step of the inner chamber. Therefore, when ER_{in} is fixed at 0.3, the CST gas reaction initially cannot be induced in the upstream segment of the inner chamber because of a relatively low fuel concentration, but it is sustained in the holes because of support from fuel and radicals from the outer chamber. When the fuel concentration in the outer chamber increases, the corresponding flame speed increases. However, when ER_{out} is 0.6, flash back is prone to occur because of the absence of the flame anchoring mechanism on the upstream segment of the outer chamber. By contrast, when ER_{out} is fixed

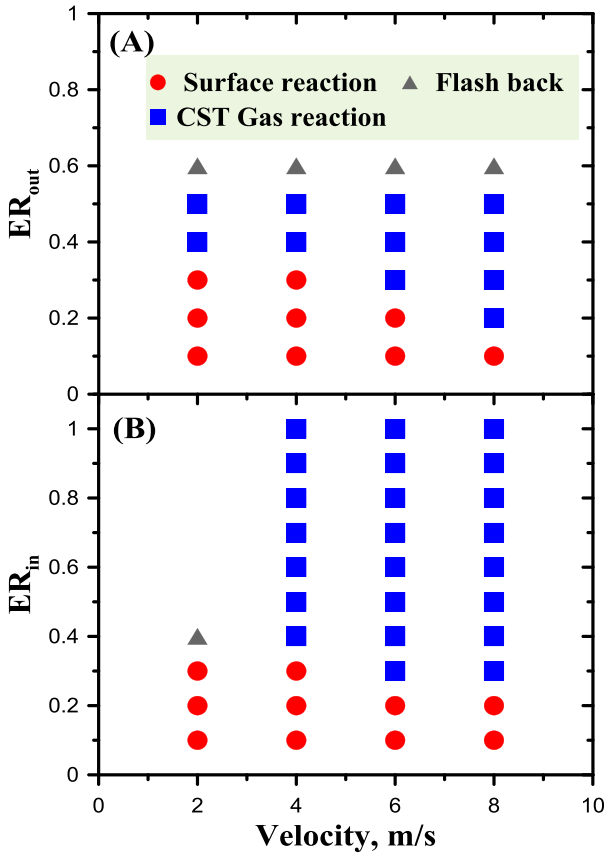

Fig. 9 – Operating ranges under (A) the different equivalence ratios of the outer chamber and the inner equivalence ratio of 0.3. (B) the different equivalence ratios of the inner chamber and the outer equivalence ratio of 0.3.

at 0.3, only the surface reaction occurs in the outer chamber. The CST gas reaction is induced in the upstream segment of the inner chamber as the fuel concentration in the inner chamber increases. Flames are supposed to be anchored in the holes or backward-facing step. When ER_{in} increases, flames do not easily flash back because of the presence of the backward-facing step in the inner chamber. This causes the wide operating range of the CST gas reaction for a fixed ER_{out} and various ER_{in} values. However, an objective of the study was to anchor the flame in the outer chamber and simultaneously integrate the radiation from flames and the platinum tube so that the radiation efficiency of the micro TPV system could be improved. Delivering a relatively high hydrogen concentration to the outer chamber is a pragmatic and feasible approach to inducing and sustaining flames on the outer surface of the micro TPV reactor.

Effect of flow velocity

To clarify the effect of flow velocity in the inner and outer chambers, various ratios of inner flow velocity to outer flow velocity, 0.5 (3/6, m/s), 1 (4.5/4.5, m/s), 1.5 (5.4/3.6, m/s), and 2 (6/3, m/s), were employed to investigate the flame behaviors under an identical total amount of fuel injection. In general, a UV-sensitive camera (most certainly intensified) was used to collect OH^* chemiluminescence using a band-pass filter around 309 nm for detecting flame position. Otherwise, planar laser-induced fluorescence of the OH radical (OH-LIF) were employed to observe the gas reaction along the micro-channel [35–37]. However, in this study it is quintessentially difficult to observe the gas reaction along the tubular reactor with photography or laser diagnostics. Owing to inherent deficiencies of the present TPV-reactor configuration and lacks of OH-LIF measuring technique, it is plausible solutions to classify the combustion characteristic of micro-TPV reactor via the observation of flame feature. Fig. 10 shows the combustion behaviors at the flow velocity ratios of 2 and 0.5 with the inner and outer equivalence ratios of 0.3. For a flow velocity ratio of 2, representing that the inner flow velocity is greater than the outer flow velocity, flames seem to be anchored in the holes, and the micro TPV exhibits bright luminescence in the upstream segment but dim luminescence in the downstream segment, as shown in Fig. 10a. Conversely, for a flow velocity ratio of 0.5, flames are anchored in the holes, and the luminescence is bright in the downstream segment but dim in the upstream segment. These results demonstrate that the CST gas reaction can be induced at two flow velocity ratios, but the flame anchoring location is apparently different. To understand the effect of flow velocity on the flame stabilization location, a simplified simulation was performed. Fig. 11 illustrates the distributions of temperature with overlaid velocity vectors and velocity magnitude level lines for flow velocity ratios of (a) 2 and (b) 0.5 at a fixed ER_{in} and ER_{out} of 0.3 within the first 1 cm from the inlet. Fig. 12 depicts the distribution of the OH mass fraction with overlaid LER level lines for velocity ratios of (a) 2 and (b) 0.5. According to the results of the numerical simulation, the mixture in the outer chamber flows toward the inner chamber regardless of the V_{in}/V_{out} condition, as shown in Fig. 11. The primary reason is that the surface-reaction-induced thermal

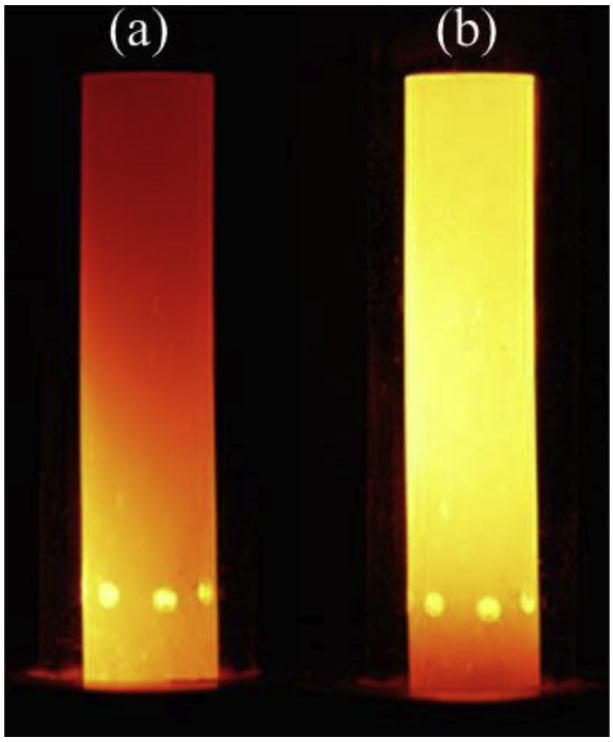

Fig. 10 – Combustion behavior under the ratios of inner velocity to outer velocity of (a) 2 and (b) 0.5 with the inner and outer equivalence ratio of 0.3.

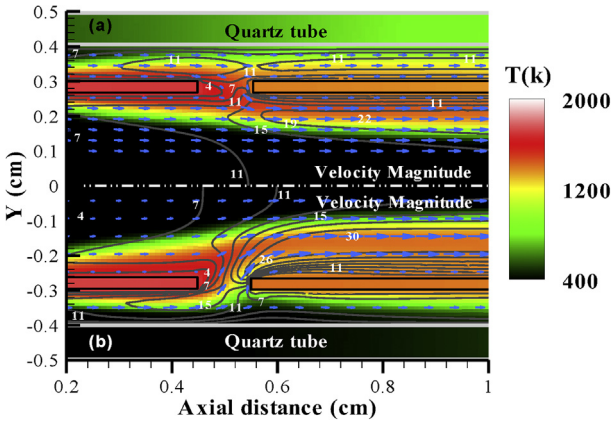

Fig. 11 – The distributions of temperature with overlaid velocity vectors and velocity magnitude level lines behavior under the ratios of inner velocity to outer velocity of (a) 2 and (b) 0.5 with the inner and outer equivalence ratio of 0.3 in first 1 cm distance away from the inlet.

expansion of the mixture in the outer chamber propels the mixture toward the inner chamber through the gap because of the narrow space in the outer chamber in comparison with that in the inner chamber. Therefore, even though the outer velocity is lower than the inner velocity, indicating that the hydrogen amount is greater in the inner chamber, the fuel in outer chamber still flows to the inner chamber through the gap. The results elucidate that the flow motion in the vicinity

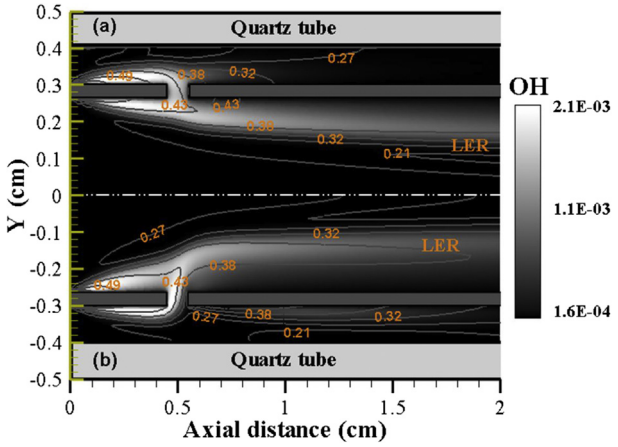

Fig. 12 – The distributions of OH mass fractions with overlaid velocity vectors and local equivalence ratio level lines under the ratios of inner velocity to outer velocity of (a) 2 and (b) 0.5 with the inner and outer equivalence ratio of 0.3 in first 2 cm distance away from the inlet.

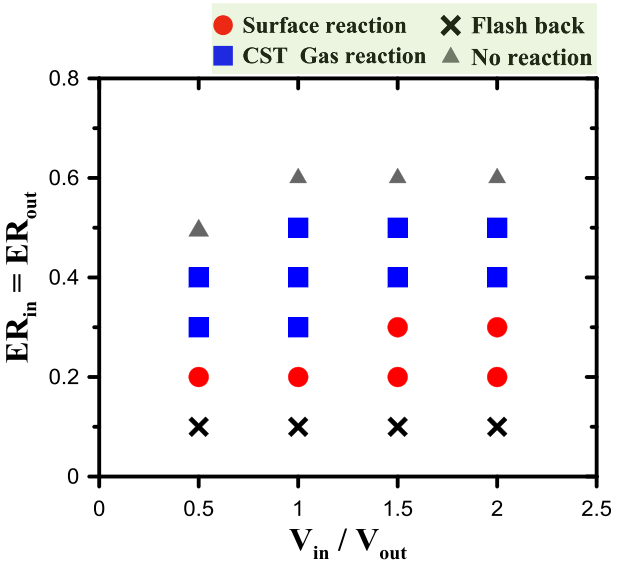

Fig. 13 – The operating range under different ratios of inner flow velocity to outer flow velocity.

of the gap is predominantly driven not by thermal diffusion and mass diffusion, but by pressure-driven flow dynamics. Furthermore, Fig. 12 indicates the distribution of the OH radical concentration, showing flame anchoring in the gap between tubes. At the flow velocity ratio of 2, the flame seems to tail toward only the inner surface of the downstream platinum tube. The flow tendency in the gap lowers the fuel concentration in the outer chamber. A low LER along the outer surface of the downstream platinum tube leads to a fuel concentration that is insufficient to induce the CST gas reaction, but is sufficient to induce the surface reaction. By contrast, at the flow velocity ratio of 0.5, the flame seems to tail toward the inner and outer surfaces of the downstream platinum tube. The outer velocity is relatively higher than the inner velocity, indicating that the hydrogen amount is greater in the outer chamber than in the inner chamber. Even the fuel/air mixture in the outer chamber still flows toward the inner chamber. The remaining fuel in the outer chamber is sufficient to induce the CST gas reaction in the downstream segment. Thus, these observations explain the differences in flame stabilization and high luminescence in Fig. 10.

Fig. 13 shows the operating range at different ratios of inner flow velocity to outer flow velocity. The stable CST gas reaction in a lower V_{in}/V_{out} condition tends toward lower equivalence ratios, whereas the stable CST gas reaction in a higher V_{in}/V_{out} condition tends toward higher equivalence ratios. In principle, the occurrence of the CST gas reaction in the inner chamber is associated with the chemical reactivity in the outer chamber. Sufficient chemical exothermicity in the outer chamber could compensate for the radiative thermal loss of the platinum tube through the quartz tube and simultaneously facilitate the induction of the CST gas reaction in the inner chamber. Regardless of the V_{in}/V_{out} condition, the mixture in the outer chamber flows toward the inner chamber. Consequently, reactors with high V_{in}/V_{out} ratios require relatively rich fuel/air mixtures to sustain the CST gas reaction in the inner chamber in order to overcome the fuel concentration reduction and the heat loss in the outer chamber. However, low V_{in}/V_{out} ratios can easily sustain the CST gas reaction in the inner chamber when the fuel/air mixture is lean. Nonetheless, when the equivalence ratio in the case of a low V_{in}/V_{out} ratio increases, the CST gas reaction is subject to blow out because of increased flame speed deteriorating the flame stabilization mechanism in the holes in the outer chamber. When the flow velocity ratio equals unity, the operating range of the CST gas reaction is wide in various equivalence ratio conditions. Accordingly, the effect of flow velocity is associated with the occurrence of the CST gas reaction in the outer chamber, but not in the inner chamber.

Demonstration of micro TPV power system

Irradiance of micro TPV power system

The overall efficiency of a TPV power system is related to the radiation efficiency of the emitter and quantum efficiency of the TPV cell. A common approach to determining the irradiance of a TPV power system is to use a single radiometer, particularly because the irradiance distribution over the micro TPV reactor is never uniform. Perturbations of combustion and fluid dynamics may lead to non-uniformity of the TPV radiation. Therefore, to mitigate the uncertainty of irradiance measurement, the proposed micro TPV reactor was placed in the center of the integrating sphere. As the radiation of the combustor scattered uniformly inside the integrating sphere, an optical fiber was used to collect the radiation and sent the signal to the spectrometer to measure the irradiance. Table 1 shows the irradiance and the corresponding radiance efficiency at different equivalence ratios of the fuel/air mixture with the fixed velocity of 6 m/s. The radiance efficiency is the ratio of the measured irradiance to the thermal energy

Table 1 – Irradiance and the corresponding radiance efficiency at different equivalence ratios of the mixture with a fixed velocity of 6 m/s.

Fuel/Air Mixtures	Irradiance (W/m^2)	Radiation efficiency (%)
H_2 ($ER_{in} = 0.3$, $ER_{out} = 0.3$)	1993	0.79
H_2 ($ER_{in} = 0.4$, $ER_{out} = 0.3$)	4453	1.42
H_2 ($ER_{in} = 0.5$, $ER_{out} = 0.3$)	5162	1.46
H_2 ($ER_{in} = 0.3$, $ER_{out} = 0.4$)	4666	1.43
H_2 ($ER_{in} = 0.3$, $ER_{out} = 0.5$)	6123	1.51

absorbed by the platinum tube. The absorbed thermal energy is associated with the surface temperature of the platinum reactor, and the surface temperature along the platinum tube (TPV reactor) was determined using the IR detector. Two scenarios were considered: the first was a fixed fuel concentration in the inner chamber, and the second was a fixed fuel concentration in the outer chamber. Regardless of the scenario, the irradiance of the TPV reactor evidently increased as the hydrogen concentration increased. In addition, the maximal irradiance was 6123 W/m^2 and the corresponding radiance efficiency was 1.51% for an ER_{in} of 0.3 and ER_{out} of 0.5.

Electrical output of micro TPV power system

To evaluate the benefit of improving the proposed micro TPV reactor, photovoltaic cells were employed to collect luminosity and convert it into electricity. However, an appropriate selection of photovoltaic for combustion-driven TPV system is associated with electrical output and the overall efficiency. It is essential to detect the spectrum distribution of radiant from the emitter and match up the quantum efficiency of photovoltaic cell. In the study, the monochromator (DK240, Spectral Products Company) with IR photoresistor (AD131-USB, Spectral Products Company) was used to measure the spectral distribution of the emitter, ranging from 400 to 1500 nm. Fig. 14 demonstrated the spectrum distribution of micro-TPV reactor with the condition of a fixed ER_{in} of 0.3 and various ER_{out} of 0.3, 0.4 and 0.5. The major radiation located in the range from 700 to 1500 nm is of interest. In general, Si PV cells can convert photons with the wavelength of 300–1100 nm, whereas GaSb PV cells can convert photons with the wavelength of 400–1800 nm. For maximizing the electrical output of PV cells, the GaSb PV cells were selected for the micro-TPV power system. Accordingly, the prototype TPV system comprised the proposed micro TPV reactor with the necessary assemblies surrounded by a GaSb PV cell array, fabricated by JX Crystal Company, as shown in Fig. 15. The TPV circuit consists of 24 gallium antimonide PV cells. Each cell array had an area of 18 cm^2 and contained two strings of six series-connected cells in tandem. The open circuit voltage (V_{oc}) and short circuit current density (I_{sc}) of the TPV panel are 23.023 V and 2.9875 A/cm^2, respectively, and the fill factor is 0.733.

Fig. 16 shows the I–V curve at different equivalence ratios and the velocity of 6 m/s. Most energy released by fossil fuel is not absorbed by the emitter and converted to irradiance. Based on the irradiation of the emitter, the effective power efficiency (η_e) is defined as the ratio of the output power to the

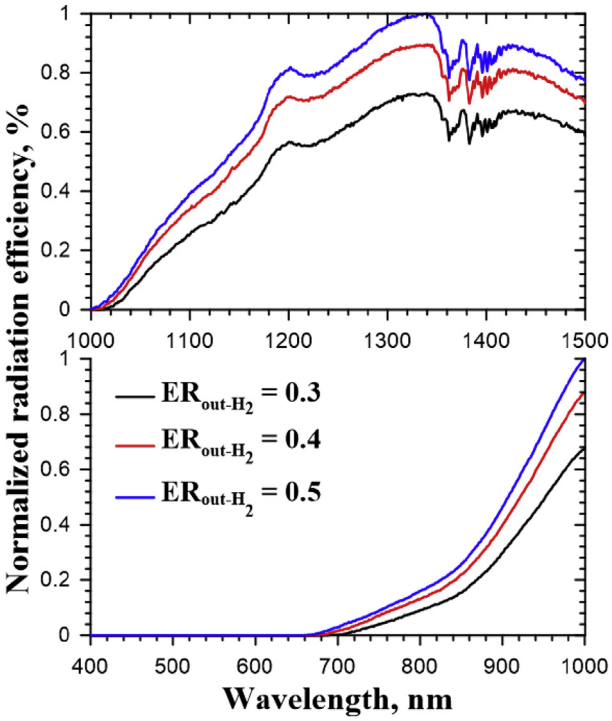

Fig. 14 – Spectrum distribution for H_2-fulled micro-TPV reactor (400–1500 nm).

Fig. 15 – The micro-TPV reactor with GaSb PV cell array.

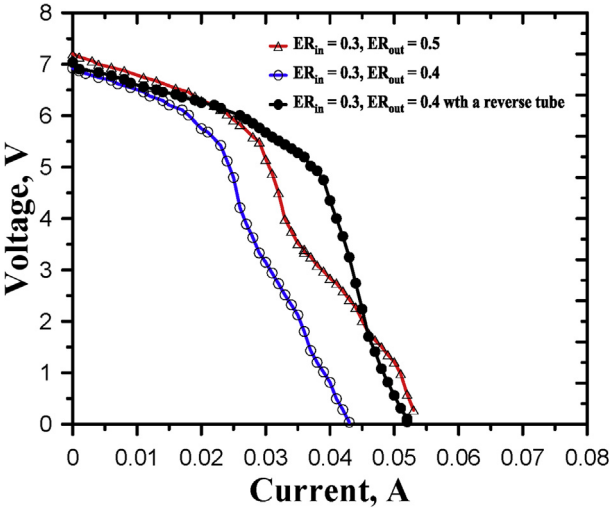

Fig. 16 – I–V curves for various equivalence ratios.

radiation power. When ER_{in} was 0.3 and ER_{out} is 0.4, the maximal power output reached 0.124 W with the corresponding η_e of 1.08%. When ER_{in} was 0.3 and ER_{out} was 0.5, the maximal power was 0.16 W with the corresponding η_e of 1.13%. However, when a reverse tube was used to redirect hot flue gas and further heated the platinum tube, the I–V performance for an ER_{in} of 0.3 and ER_{out} of 0.4 was substantially improved, and the maximal power output was 0.187 W with the corresponding η_e of 1.56%. Nonetheless, flash back occurred when ER_{in} is 0.3 and ER_{out} is 0.5.

Conclusion

The flame stabilization mechanism of a micro TPV reactor was investigated through a simplified numerical case of two platinum segments in tandem. The function of the gap between the two platinum tubes in tandem was addressed by analyzing the fuel concentration and flow velocity effects. In addition, a platinum tube with a ring of holes was fabricated and tested in a series of experiments. The radiation efficiency and effective power efficiency of the micro TPV power system were measured under various experimental conditions. The most crucial results are listed as follows:

1. It is apparently difference of luminous intensity and temperature distribution of emitter surface in different hydrogen/air deployments. The speculation is that the effect of fuel concentration in two sides of chambers impacts the flame stabilization. Numerical results demonstrated the velocity vectors in the vicinity of the gap flow from the outer chamber to the inner chamber due to the localized pressure imbalance between the two sides of the gap. The tendency of unburnt fuels to be drawn to the inner chamber lowers the concentration of remaining fuel in the outer chamber. Therefore, insufficient heat release and the remaining fuel cannot sustain the consequent chemical reaction in the downstream segment of the outer chamber.
2. The occurrence of the CST gas reaction in the inner chamber is associated with the chemical reactivity in the outer chamber. Regardless of the V_{in}/V_{out} condition, the mixture in the outer chamber flows toward the inner chamber. Consequently, reactors with high V_{in}/V_{out} ratios require relatively rich fuel/air mixtures to sustain the CST gas reaction in the inner chamber in order to overcome the fuel concentration reduction and the heat loss in the outer chamber. On the contrary, low V_{in}/V_{out} ratios can easily sustain the CST gas reaction in the inner chamber when the fuel/air mixture is lean.
3. An integrating sphere connected to a spectrometer was employed to measure the irradiation of the emitter. The emitter was placed in the center of the integrating sphere, and the spectrometer was connected to the integrating sphere to obtain the radiation flux. The irradiance of the TPV reactor evidently increased as the hydrogen concentration increased. In addition, the maximal irradiance was 6123 W/m^2 and the corresponding radiance efficiency was 1.51% for an ER_{in} of 0.3 and ER_{out} of 0.5.
4. For the overall efficiency of the TPV system, the maximal power was 0.16 W with the corresponding η_e of 1.13% as ER_{in} was 0.3 and ER_{out} was 0.5. However, when a reverse tube is used to redirect hot flue gas and further heat the platinum tube, the I–V performance for an ER_{in} of 0.3 and ER_{out} of 0.4 was substantially improved, and the maximal power output was 0.19 W with the corresponding η_e of 1.56%.

Acknowledgements

This research was partially supported by the Ministry of Science and Technology under Grant Nos. MOST 104-2228-E-006-012 and MOST 105-2628-E-006-005-MY3. Computer time and numerical packages provided by the National Center for High-Performance Computing, Taiwan, are gratefully acknowledged.

REFERENCES

[1] Dunn-Rankin D, Leal EM, Walther DC. Personal power systems. Prog Energy Combust Sci 2005;31:422–65.
[2] Kyritsis DC, Roychoudhury S, McEnally CS, Pfefferle LD, Gomez A. Mesoscale combustion: a first step towards liquid fueled batteries. Exp Therm Fluid Sci 2004;28:763–70.
[3] Fernandez-Pello AC. Micropower generation using combustion: issues and approaches. Proc Combust Inst 2002;29:883–99.
[4] Epstein AH. Millimeter-scale, micro-electro-mechanical systems gas turbine engines. J Eng Gas Turbines Power 2004;126:205–26.
[5] Aichlmayr HT, Kittelson DB, Zachariah MR. Micro-HCCI combustion: experimental characterization and development of a detailed chemical kinetic model with coupled piston motion. Combust Flame 2003;135:227–48.
[6] Yadav S, Yamasani P, Kumar S. Experimental studies on a micro power generator using thermo-electric modules mounted on a micro-combustor. Energy Convers Manag 2015;99:1–7.
[7] Chou SK, Yang WM, Chua KJ, Li J, Zhang KL. Development of micro power generators – a review. Appl Energy 2011;88:1–16.
[8] Li YH, Lien YS, Chao YC, Dunn-Rankin D. Performance of a mesoscale liquid fuel-film combustion-driven TPV power system. Prog Photovoltaics 2009;17:327–36.
[9] Li YH, Li HY, Dunn-Rankin D, Chao YC. Enhancing thermal, electrical efficiencies of a miniature combustion-driven thermophotovoltaic system. Prog Photovoltaics 2009;17:502–12.
[10] Qiu K, Hayden ACS. Development of a novel cascading TPV and TE power generation system. Appl Energy 2012;91:304–8.
[11] Butcher TA, Hammonds JS, Horne E, Kamath B, Carpenter J, Woods DR. Heat transfer and thermophotovoltaic power generation in oil-fired heating systems. Appl Energy 2011;88:1543–8.
[12] Yang WM, Chou SK, Shu C, Li ZW, Xue H. Combustion in micro-cylindrical combustors with and without a backward facing step. Appl Therm Eng 2002;22:1777–87.
[13] Wan J, Fan A, Yao H, Liu W. Flame-anchoring mechanisms of a micro cavity-combustor for premixed H2/air flame. Chem Eng J 2015;275:17–26.
[14] Sui R, Prasianakis NI, Mantzaras J, Mallya N, Theile J, Lagrange D, et al. An experimental and numerical investigation of the combustion and heat transfer characteristics of hydrogen-fueled catalytic microreactors. Chem Eng Sci 2016;141:214–30.

[15] Pan JF, Huang J, Li DT, Yang WM, Tang WX, Xue H. Effects of major parameters on micro-combustion for thermophotovoltaic energy conversion. Appl Therm Eng 2007;27:1089–95.
[16] Leu C-H, King S-C, Huang J-M, Chen C-C, Tzeng S-S, Lee C-I, et al. Visible images of the catalytic combustion of methanol in a micro-channel reactor. Chem Eng J 2013;226:201–8.
[17] Li Y-H, Chen G-B, Wu F-H, Cheng T-S, Chao Y-C. Combustion characteristics in a small-scale reactor with catalyst segmentation and cavities. Proc Combust Inst 2013;34:2253–9.
[18] Ahn J, Eastwood C, Sitzki L, Ronney PD. Gas-phase and catalytic combustion in heat-recirculating burners. Proc Combust Inst 2005;30:2463–72.
[19] Li Y-H, Chen G-B, Wu F-H, Cheng T-S, Chao Y-C. Effects of catalyst segmentation with cavities on combustion enhancement of blended fuels in a micro channel. Combust Flame 2012;159:1644–51.
[20] Li YH, Chen GB, Hsu HW, Chao YC. Enhancement of methane combustion in microchannels: effects of catalyst segmentation and cavities. Chem Eng J 2010;160:715–22.
[21] Yang WM, Chou SK, Shu C, Li ZW, Xue H. Study of catalytic combustion and its effect on microthermophotovoltaic power generators. J Phys Appl Phys 2005;38:4252.
[22] Sui R, Mantzaras J. Combustion stability and hetero-/homogeneous chemistry interactions for fuel-lean hydrogen/air mixtures in platinum-coated microchannels. Combust Flame 2016;173:370–86.
[23] Wu Y-T, Li Y-H. Combustion characteristics of a micro segment platinum tubular reactor with a gap. Chem Eng J 2016;304:485–92.
[24] Yang WM, Chou SK, Shu C, Li ZW, Xue H. Development of microthermophotovoltaic system. Appl Phys Lett 2002;81:5255–7.
[25] Li Y-H, Chen G-B, Cheng T-S, Yeh Y-L, Chao Y-C. Combustion characteristics of a small-scale combustor with a percolated platinum emitter tube for thermophotovoltaics. Energy 2013;61:150–7.
[26] Jiang D, Yang W, Chua KJ, Ouyang J. Thermal performance of micro-combustors with baffles for thermophotovoltaic system. Appl Therm Eng 2013;61:670–7.
[27] Park JH, Lee SI, Wu H, Kwon OC. Thermophotovoltaic power conversion from a heat-recirculating micro-emitter. Int J Heat Mass Transf 2012;55:4878–85.
[28] Lei Y, Chen W, Lei J. Combustion and direct energy conversion inside a micro-combustor. Appl Therm Eng 2016;100:348–55.
[29] Yang WM, Siawkiang C, Chang S, Hong X, Li ZW. Effect of wall thickness of micro-combustor on the performance of micro-thermophotovoltaic power generators. Sensor Actuator Phys 2005;119:441–5.
[30] Yang WM, Chou SK, Shu C, Xue H, Li ZW. Research on micro-thermophotovoltaic power generators with different emitting materials. J Micromech Microeng 2005;15:S239–42.
[31] Beder EC, Bass CD, Shacklef WL. Transmissivity and absorption of fused quartz between 0.22mu and 3.5mu from room temperature to 1500 degree C. Appl Optic 1971;10. 2263-&.
[32] Li Y-H, Cheng T-S, Lien Y-S, Chao Y-C. Development of a tubular flame combustor for thermophotovoltaic power systems. Proc Combust Inst 2011;33:3439–45.
[33] Miller JA, Bowman CT. Mechanism and modeling of nitrogen chemistry in combustion. Prog Energy Combust Sci 1989;15:287–338.
[34] Deutschmann O, Maier LI, Riedel U, Stroemman AH, Dibble RW. Hydrogen assisted catalytic combustion of methane on platinum. Catal Today 2000;59:141–50.
[35] Appel C, Mantzaras J, Schaeren R, Bombach R, Inauen A, Kaeppeli B, et al. An experimental and numerical investigation of homogeneous ignition in catalytically stabilized combustion of hydrogen/air mixtures over platinum. Combust Flame 2002;128:340–68.
[36] Reinke M, Mantzaras J, Schaeren R, Bombach R, Inauen A, Schenker S. High-pressure catalytic combustion of methane over platinum: in situ experiments and detailed numerical predictions. Combust Flame 2004;136:217–40.
[37] Qin Z, Lissianski VV, Yang H, Gardiner WC, Davis SG, Wang H. Combustion chemistry of propane: a case study of detailed reaction mechanism optimization. Proc Combust Inst 2000;28:1663–9.